Destabilization of the $m = 1$ Diocotron Mode in Non-neutral Plasmas

John M. Finn* and Diego del-Castillo-Negrete
Theoretical Division, Los Alamos National Laboratory, Los Alamos, New Mexico 87545

Daniel C. Barnes
Applied Theoretical and Computational Division, Los Alamos National Laboratory, Los Alamos, New Mexico 87545
(Received 17 May 1999)

The theory for a Penning-Malmberg trap predicts $m = 1$ diocotron stability. However, experiments with hollow profiles show robust exponential growth. We propose a new mechanism of destabilization of this mode, involving parallel compression due to end curvature. The results are in good agreement with the experiments. The resulting *modified drift-Poisson equations* are analogous to the geophysical shallow water equations, and conservation of line integrated density corresponds to that of potential vorticity. This analogy predicts Rossby waves in non-neutral plasmas and an $m = 1$ instability in fluids.

PACS numbers: 52.25.Wz, 47.20.Cq, 47.20.Ft, 52.35.–g

Diocotron instabilities in magnetically confined non-neutral plasmas (e.g., in Penning-Malmberg traps [1]) are $\mathbf{E} \times \mathbf{B}$ drift modes which are analogous to shear flow instabilities in fluids. According to linear theory [2,3], modes with $m > 1$ can be unstable for hollow (nonmonotonic) density profiles, but for $m = 1$ there are no unstable diocotron modes. However, experiments on a Penning-Malmberg trap (see Fig. 1) confining electrons with a hollow density profile show a robust exponential $m = 1$ instability [4].

The theory of diocotron modes is based on the drift-Poisson model [3], which is valid for low frequency and for low density. This system consists of the continuity equation with the velocity given by the $\mathbf{E} \times \mathbf{B}$ drift and the potential obtained from the Poisson equation, i.e.,

$$\frac{Dn}{Dt} = 0\,, \qquad \mathbf{u}_\perp = \frac{\hat{\mathbf{z}} \times \nabla\phi}{B_0}\,, \qquad \nabla_\perp^2 \phi = 4\pi e n\,, \tag{1}$$

where $D/Dt \equiv \partial/\partial t + \mathbf{u}_\perp \cdot \nabla$, and $-e$ is the electron charge. Because B_0 is uniform, the diamagnetic drift $\mathbf{u}_D \equiv \hat{\mathbf{z}} \times \nabla P/neB_0$ makes no contribution in the continuity equation, i.e., $\nabla \cdot (n\mathbf{u}_D) = 0$. There have been several attempts to explain the $m = 1$ instability observed in the experiments [4]. Smith and Rosenbluth [5] have used (1) to show algebraic growth, $\phi \sim \sqrt{t}$, related to phase mixing at the end point of the continuum, where the $\mathbf{E} \times \mathbf{B}$ rotation velocity $\Omega(r)$ is maximum. This growth is inconsistent with the exponential growth measured in the experiment. Smith [6] has shown that a modification to (1) can lead to exponential growth for $m = 1$. However, because of the phenomenological nature of the model, it has not been possible to compare these results with the experiments. In Refs. [7,8] it was shown that finite Larmor radius effects can also lead to instability, but with growth rates smaller than those observed in the experiments by several orders of magnitude.

Here we resolve this discrepancy between theory and experiment in terms of the *modified drift-Poisson model* of Ref. [9]. This model is based on the theoretical observation that in general the ends of a plasma confined in a Penning-Malmberg trap are curved. In Fig. 2 we show contours of $\phi(r, z) - \phi_0(r)$, where $\phi_0(r)$ is the potential in the central Debye shielded region. Equilibria with uniform temperature T are solutions to the equation $\nabla_\perp^2 \phi = 4\pi e n_0(r) \exp[e(\phi - \phi_0)/T]$ with $r^{-1}(d/dr)(rd\phi_0/dr) = 4\pi e n_0(r)$. A typical particle reflects axially, where $e[\phi(r, z) - \phi_0(r)] = -T$. Equilibrium computations as in Refs. [10–12] show that the length decreases with r, and this effect is stronger for large $\phi_0(r = 0)/V$, where V is the end-cap potential. For typical values of $\phi_0(r = 0)/V$ the equilibrium half length $L_0(r)$ of the plasma can be parametrized by

$$L_0(r) = L_0(0)\,(1 - \kappa r^2)\,, \tag{2}$$

with κ typically positive and $L_0(0) \approx L_c$ (cf. Fig. 1). This description is an idealization of zero Debye length, in which all particles are assumed to reflect at $z = L_0(r)$, and n and ϕ are independent of z for $-L_0(r) < z < L_0(r)$. This idealization neglects phenomena associated with axial thermal motion [13,14], effects which are important on a much longer time scale than those considered here. The region $|z| > L_0(r)$ is taken to be vacuum.

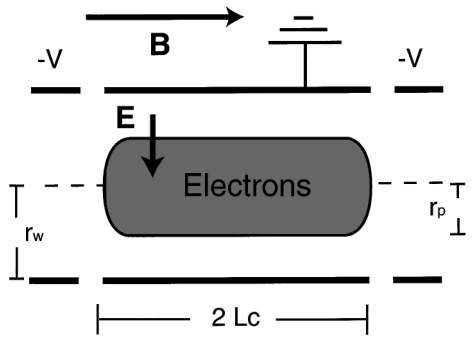

FIG. 1. Schematic diagram of the cylindrical plasma confinement device. The middle cylinder at $r = r_w$ has length L_c and is grounded. The potential at the end caps is $-V$. From Ref. [9].

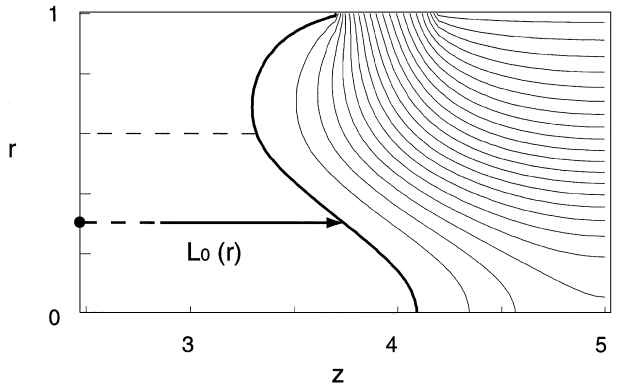

FIG. 2. Potential difference $\phi(r,z) - \phi_0(r)$, obtained for the density profile in (6) with $\mu = 3$, $\phi_0(0)/V = 0.75$. The dashed line shows the plasma radius r_p, with $L_0'(r) < 0$ for $r < r_p$. From Ref. [9].

The modified drift-Poisson equations are derived by integrating in z the continuity equation including parallel compression $\partial(nu_z)/\partial z$ over $-L(r,\theta,t) < z < L(r,\theta,t)$. This yields $Dn/Dt + n[u_z(L) - u_z(-L)]/2L = 0$, and using the relations $u_z(r,\theta,L) = (D/Dt)L$, $u_z(r,\theta,-L) = -(D/Dt)L$ we find

$$\frac{D}{Dt}(nL) = 0. \tag{3}$$

The quantity nL is the *line integrated density,* and Eq. (3) expresses charge conservation of plasma columns aligned with **B**. Because the relevant quantities are independent of z for $-L < z < L$, the Poisson equation is as in Eq. (1). In general we can write $L(r,\theta,t) = L_0(r) + \tilde{\Lambda}[\phi(r,\theta,t) - \phi_0(r)]$, where $\tilde{\Lambda}$ is obtained by coupling the plasma to the vacuum. Using Poisson's equation we can write Eq. (3) as

$$\frac{D}{Dt}\nabla_\perp^2\phi + \frac{\nabla_\perp^2\phi}{L}\left(-\frac{L_0'}{r}\frac{\partial\phi}{\partial\theta} + \frac{D}{Dt}\tilde{\Lambda}\right) = 0, \tag{4}$$

where prime denotes d/dr. Parallel compression and expansion enter in Eq. (4) in the last term and correspond to changes in the length of plasma columns aligned with **B**. There is a conducting wall at $r = r_w$, and all quantities are in dimensionless form with lengths scaled to the wall radius r_w, velocities to $\omega_{pe}^2/\Omega_{ce}$, and potential to $4\pi\overline{n}er_w^2$, where $\overline{n}$ is the average density. Equation (4) with $\tilde{\Lambda} = 0$ is analogous to the shallow water equations [15] of geophysical fluid dynamics, and the line integrated density nL is the analog of the potential vorticity [16]. The first term in the brackets, which is due to curvature, is the analog of the term in the β-plane approximation [15] due to topography variation or to latitude variation of the Coriolis force.

Linearizing Eq. (4) and assuming normal mode dependence $\tilde{\phi} \sim e^{im\theta - i\omega t}$, we obtain

$$\nabla_\perp^2\tilde{\phi} + \frac{m(n_0L_0)'}{r[\omega - m\Omega(r)]L_0}\tilde{\phi} + n_0\frac{\tilde{\Lambda}[\tilde{\phi}]}{L_0} = 0, \tag{5}$$

where $\Omega(r)$ is the equilibrium rotation velocity. This equation becomes the Rayleigh equation when L_0' and $\tilde{\Lambda}$ are zero. The second term on the left is responsible for Rossby waves in non-neutral plasmas [16].

Consider density profiles of the form

$$n_0(r) = n_0(0)[1 - (r/r_p)^2]^2[1 + (\mu + 2)(r/r_p)^2] \tag{6}$$

for $0 < r \le r_p$ and zero otherwise, as used in Refs. [9,17]. Here, r_p is the plasma radius, and μ is the hollowness parameter. For $\mu > 0$ the maximum of $n_0(r)$ is at $r = r_n > 0$, and the maximum $\Omega_{\max}$ of $\Omega(r)$ is at $r = r_\Omega$, with $0 < r_n < r_\Omega$.

Ignoring free boundary effects ($\tilde{\Lambda} = 0$), and using Eq. (2), Eq. (5) takes the form

$$(\omega - m\Omega)\nabla_\perp^2\tilde{\phi} + \frac{m}{r}\left[n_0' - \left(\frac{2\kappa r}{1 - \kappa r^2}\right)n_0\right]\tilde{\phi} = 0. \tag{7}$$

As discussed in Refs. [5,6], for $\kappa = 0$ there is a weak neutral mode

$$\tilde{\phi}_0(r) = r[\omega - \Omega(r)]\Theta(r_\Omega - r), \tag{8}$$

where $\Theta(r_\Omega - r)$ is a step function displacement, with $\omega = \Omega_{\max}$, the end point of the continuum.

Figure 3 shows the growth rate γ for $\kappa > 0$ obtained using Eqs. (7) and (6) for $\mu = 3$, $r_p = 0.59$. The growth rate γ scales as $\kappa^{2/3}$ for κ small, similar to the scaling obtained in [6]. The fractional power and zero instability threshold in κ are associated with a boundary layer near $r = r_\Omega$ related to the singularity in the neutral mode of Eq. (8) there. The real frequency ω_r decreases slowly from $\Omega_{\max}$ as κ is increased. The potential for κ small is similar to that of Eq. (8), but it is smooth, has a zero just inside $r = r_\Omega$, and goes to zero rapidly in the region $r > r_\Omega$. For $\kappa < 0$ the mode remains stable (again with $\tilde{\phi}$ smooth but with no zero in the interval $0 < r < r_\Omega$) with pure real frequency $\omega = \omega_r$ that increases above $\Omega_{\max}$ as $|\kappa|$ increases. That is, the stable mode for $\kappa < 0$ becomes nonresonant. The physical mechanism for this instability involves the fact that ω_r decreases as κ increases. This is because for $m = 1$ and $\kappa > 0$, compression and expansion

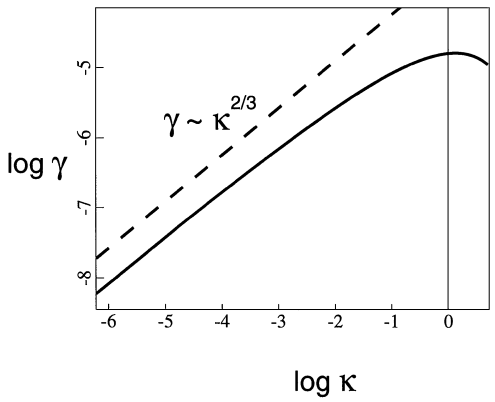

FIG. 3. Dependence of the growth rate γ on κ for $\mu = 3$ on a log-log scale, showing the dependence $\gamma \sim \kappa^{2/3}$. From Ref. [9].

parallel to **B** creates a perturbed dipole of charge. In the frame rotating with ω_r, the additional $\mathbf{E} \times \mathbf{B}$ drift due to this dipole is in the opposite direction to ω_r, decreasing ω_r. (This is essentially the physical mechanism of Rossby wave propagation in Penning traps [16].) This frequency down-shift couples the marginal mode of Eq. (8) to the plasma, and with the hollowness produces instability.

Onset for the instability is for both μ and κ equal to zero. Specifically, for $\mu \to 0$, there are scaling properties due to the localization of the mode to $r \sim r_n \sim r_\Omega$ similar to that in Eq. (8). For μ small we find $n_0(r) = 1 + C_1\rho^2 - C_2\rho^4 + O(\mu^3)$ with $\rho \equiv r/r_p$, where $C_1 = O(\mu)$ and $C_2 = O(1)$, and similarly for $\Omega(r)$. For Eq. (6), $C_1 = \mu$, $C_2 = -3$. Thus, $r_n \sim r_\Omega \sim \mu^{1/2}$. We consider Eq. (7) for r of order $\mu^{1/2}$. Defining $\delta\omega = \omega - \Omega_{\max}$, we find from Eq. (7) for $r \sim \mu^{1/2}$

$$\nabla_\perp^2 \tilde{\phi} + \frac{d/d\rho[(\mu - 3\rho^2)\rho^2 - \kappa r_p^2 \rho^2]}{\rho[\delta\omega - (\mu - 2\rho^2)\rho^2/4]}\,\tilde{\phi} = 0. \quad (9)$$

If we assume $\delta\omega \sim \mu^2$ and $\kappa \sim \mu$, we find that the terms of Eq. (9) are all of the order of μ^2. This implies the scaling

$$\delta\omega = \mu^2 \Gamma(\kappa/\mu), \qquad \tilde{\phi} = \Phi(\kappa/\mu, \rho/\sqrt{\mu}). \quad (10)$$

In Fig. 4 we show γ/μ^2 as a function of κ/μ obtained by integrating Eq. (7) for five values of μ. In agreement with Eq. (10), the curves converge to a single universal curve, with deviation of the order of μ. The scaling predicted by Eq. (10) is accurate even for fairly large μ and κ. As discussed, the results in Fig. 3 show that for $\kappa \to 0$, $\gamma \sim \kappa^{2/3}$. From Fig. 4 we observe further that the marginal stability point to the right satisfies $\kappa/\mu \approx 1.55$, with an error apparently smaller than order μ.

Equation (7) is a modified Rayleigh equation, with $(n_0 L_0)'/L_0$ taking the place of n_0'. Accordingly, the usual Rayleigh criterion [3] is easily generalized to a modified Rayleigh criterion: A sufficient condition for stability is that the line integrated density $n_0 L_0$ be monotonic. Since $L_0(r)$ [cf. Eq. (2)] is monotonically decreasing function, it follows that this condition is satisfied for κ sufficiently large. Note that the modified Rayleigh criterion applies to *all* modes with $m \neq 0$. Results with $|m| > 1$ are shown in Ref. [18].

For the free boundary case, the general equation (5) must be used. The perturbation $\tilde{\Lambda}$ is computed by matching to the vacuum region for $|z| > L(r, \theta, t)$. The continuity of the normal as well as the tangential components of the electric field at $z = L_0(r) + \tilde{\Lambda}[\tilde{\phi}]$

$$\frac{\partial}{\partial z}(\phi_0^e + \tilde{\phi}^e)|_{z=L_0(r)+\tilde{\Lambda}[\tilde{\phi}^i]} = 0 \quad (11)$$

implies to first order

$$\tilde{\Lambda}[\tilde{\phi}^i]\,\frac{\partial^2 \phi_0^e}{\partial z^2}\,\Big|_{z=L_0(r)} = -\frac{\partial \tilde{\phi}^e}{\partial z}\,\Big|_{z=L_0(r)}, \quad (12)$$

where e and i refer to exterior and interior. An alternate derivation of the matching conditions based on the perturbed density at the ends is shown in [18]. To express $\partial_z \tilde{\phi}$ at $z = L_0(r)$ in terms of $\tilde{\phi}$ at $z = L_0(r)$ involves solving Laplace's equation for $L_0(r) < z < L_0(0) + b$, where b is the length of the end cap. (See Fig. 1.) However, for $b \ll r_w = 1$, assuming $L_0(0) - L_0(r) = O(b)$, and with Neumann boundary conditions at $z = L_0(0) + b$ as an approximate open boundary condition, there is a differential approximation [9]:

$$\partial_z \tilde{\phi}^e = b f(r) \nabla_\perp^2 \tilde{\phi}^i, \quad (13)$$

where $f(r) \equiv 1 + [L_0(0) - L_0(r)]/b$. Substituting Eq. (13) in Eq. (5) we obtain

$$(\omega - m\Omega)\nabla_\perp^2 \tilde{\phi} + \frac{m[n_0' - 2\kappa r n_0/(1 - \kappa r^2)]}{r(1 + \eta + \kappa r^2)}\,\tilde{\phi} = 0, \quad (14)$$

where $\eta \equiv b/L_0(0)$. Figure 5 shows the growth rate γ as a function of η for $\mu = 3$ and for various values of κ. The differential approximation in Eq. (13) is valid for $\kappa/\eta \sim 1$ or smaller. There is a qualitative similarity between the

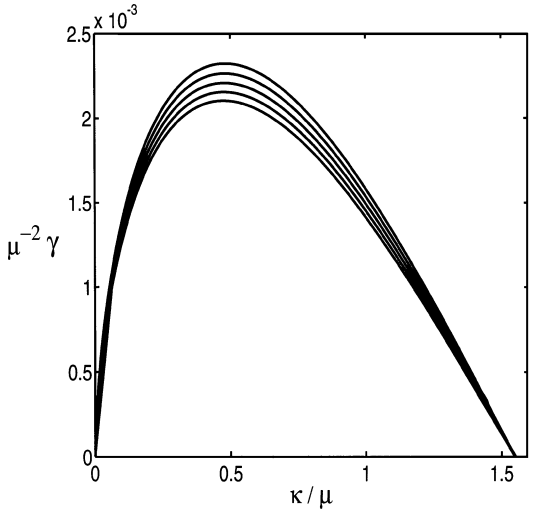

FIG. 4. Scaled growth rate γ/μ^2 as a function of κ/μ, for $\mu = 0.05$ (top curve), 0.10, 0.15, 0.20, and 0.25 (bottom curve), showing the self-similar form of Eq. (10). From Ref. [9].

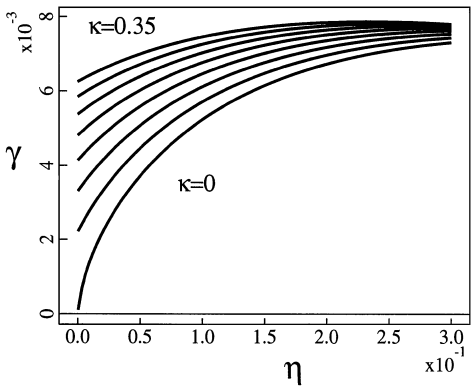

FIG. 5. Dependence of the growth rate γ on η according to Eq. (14), for seven equally spaced values of κ between 0 and 0.35 for $\mu = 3$. From Ref. [9].

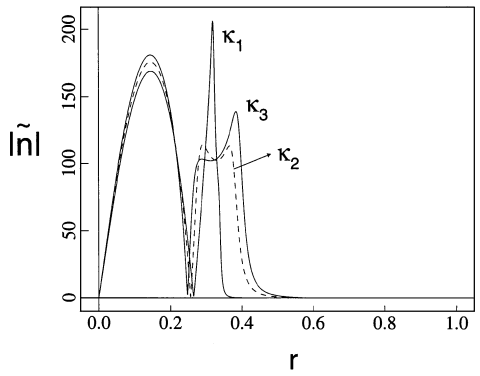

FIG. 6. Modulus of perturbed density $|\tilde{n}|$ as a function of radius for $\eta = 0$ and $\kappa_1 = 0.002$, $\kappa_2 = 0.33$, and $\kappa_3 = 0.67$. From Ref. [9].

behavior as a function of η and as a function of κ. In particular, $\gamma \sim \eta^{2/3}$ for $\kappa = 0$, $\eta > 0$, and the mode is stable and nonresonant ($\omega_r > \Omega_{\max}$) for $\kappa = 0$, $\eta < 0$.

The parameters of the experiment [4] are $\overline{n} = 5 \times 10^6$ cm^{-3}, $B_0 = 375$ G, $V = -50$ V, and central potential $\phi_0(r = 0, z = 0) \sim -18$ V. The temperature is $T = 1.2$ eV, and the plasma radius r_p is 2 cm. The total length of the trap $\sim 2L_0(0) = 30$ cm, and the conducting wall is at $r_w = 3.8$ cm. In the experiment, the real frequency of the instability ω_r is very close to the maximum value of the $\mathbf{E} \times \mathbf{B}$ rotation frequency, $\Omega_{\max} = 9 \times 10^5$ sec^{-1}, and the growth rate is $\gamma = 2.3 \times 10^4$ sec^{-1}, giving $\gamma/\omega_r = 0.025$. To compare our model with the experiment, we fixed $\mu = 3$ [$n_{\max}/n_0(0) = 1.28$] in the results of Fig. 5.

For the results shown in Fig. 5, ω_r is just below $\Omega_{\max} = 0.6$, as discussed, and for $\kappa = 0.25$, $\eta = 0.15$ we find $\gamma \sim 1.0 \times 10^{-2}$, giving $\gamma/\omega_r \sim 0.017$, in reasonable agreement with the experiment. Equilibrium results show that $\kappa \sim 0.25$ is consistent with the above experimental parameters. The value $\eta = 0.15$ was chosen to satisfy the condition $b = \eta L_0(0) < 1$. Results using a Green's function approach for $b \sim 1$ are left for a future publication. For $\kappa = 0.25$, $\eta = 0.15$, $\mu = 4$ [the latter giving $n_{\max}/n_0(0) = 1.41$], we obtain $\gamma \sim 1.2 \times 10^{-2}$, giving $\gamma/\omega_r \sim 0.020$. The self-shielding nature of the mode observed in the experiment is also in agreement with the theory: $\tilde{\phi}$ is small for $r > r_\Omega$, similar to the neutral mode of Eq. (8), for small κ, η. The perturbed density $\tilde{n}$ is shown in Fig. 6 for $\eta = 0$ and three values of κ. The density profiles shown are similar to the profiles in the experiment [4]. Finally, equilibrium results show that κ increases as the length of the plasma decreases, reaching large values $\kappa \sim 1$ for which the mode is stabilized for $L_0(0)/r_w \sim 1$. This result is consistent with experimental results showing stability for the $m = 1$ mode for short enough plasmas [19]. More recent experiments [20] show agreement with the theory over a wider range of parameters, and show specifically the decrease of ω_r and $\gamma \sim \kappa^{2/3}$ scaling for small $\kappa > 0$, the stabilization for larger κ, and the stable mode with positive ω_r for $\kappa < 0$.

In summary, we have found good agreement between our theoretical results and the experimental results [4,20], specifically concerning the growth rate and frequency of the mode, the mode structure, and stabilization for short plasmas. Furthermore, the analogy with geophysical fluid dynamics suggests the existence of Rossby waves in Penning-Malmberg traps [16] and an $m = 1$ instability in rotating fluids with sloping bottom and hollow vorticity profiles [18].

We wish to thank C. F. Driscoll, A. A. Kabantsev, and T. M. O'Neil for stimulating and useful discussions.

*Email address: finn@lanl.gov

[1] J. H. Malmberg and J. S. deGrassie, Phys. Rev. Lett. **35**, 577 (1975).
[2] R. H. Levy, Phys. Fluids **8**, 1288 (1965); **11**, 920 (1968).
[3] R. C. Davidson, *Physics of Noneutral Plasmas* (Addison-Wesley, Reading, MA, 1990).
[4] C. F. Driscoll, Phys. Rev. Lett. **64**, 645 (1990).
[5] R. A. Smith and M. N. Rosenbluth, Phys. Rev. Lett. **64**, 649 (1990).
[6] R. A. Smith, Phys. Fluids B **4**, 287 (1992).
[7] S. N. Rasband, R. L. Spencer, and R. R. Vanfleet, Phys. Fluids B **5**, 669 (1993).
[8] S. N. Rasband, Phys. Plasmas **3**, 94 (1996).
[9] J. M. Finn, D. del-Castillo-Negrete, and D. C. Barnes, Phys. Plasmas **6**, 3744 (1999).
[10] S. A. Prasad and T. M. O'Neil, Phys. Fluids **22**, 278 (1979).
[11] A. J. Peurrung and J. Fajans, Phys. Fluids B **2**, 693 (1990).
[12] R. L. Spencer, S. N. Rasband, and R. R. Vanfleet, Phys. Fluids B **5**, 4267 (1993).
[13] A. J. Peurrung and J. Fajans, Phys. Fluids B **5**, 4295 (1993).
[14] B. P. Cluggish, C. F. Driscoll, K. Avinash, and J. A. Helffrich, Phys. Plasmas **4**, 2062 (1997).
[15] R. Salmon, *Lectures on Geophysical Fluid Dynamics* (Oxford University Press, New York, 1998).
[16] D. del-Castillo-Negrete, J. M. Finn, and D. C. Barnes, in *Nonneutral Plasmas III*, edited by J. J. Bollinger *et al.*, AIP Conf. Proc. No. 498 (AIP, New York, 1999).
[17] R. C. Davidson and G. M. Felice, Phys. Plasmas **5**, 3497 (1998).
[18] J. M. Finn, D. del-Castillo-Negrete, and D. C. Barnes, in *Nonneutral Plasmas III* (Ref. [16]).
[19] C. F. Driscoll, J. H. Malmberg, and K. S. Fine, Phys. Rev. Lett. **60**, 1290 (1988).
[20] A. A. Kabantsev and C. F. Driscoll, in *Nonneutral Plasmas III* (Ref. [16]).